Spin and orbital states in single-layered $La_{2-x}Ca_xCoO_4$ studied by doping- and temperature-dependent near-edge x-ray absorption fine structure

M. Merz,[1,*] D. Fuchs,[1] A. Assmann,[1,2] S. Uebe,[1,2] H. v. Löhneysen,[1,3] P. Nagel,[1] and S. Schuppler[1]

[1]*Institut für Festkörperphysik, Karlsruhe Institute of Technology, D-76021 Karlsruhe, Germany*

[2]*Fakultät für Physik, Karlsruhe Institute of Technology, D-76031 Karlsruhe, Germany*

[3]*Physikalisches Institut, Karlsruhe Institute of Technology, D-76031 Karlsruhe, Germany*

(Received 17 February 2011; published 29 July 2011)

The doping-dependent valence, orbital, and spin-state configurations of single-layered $La_{2-x}Ca_xCoO_4$ ($x = 0$, 0.5, 1, and 1.5) were investigated with temperature-dependent near-edge x-ray absorption fine structure at the Co $L_{2,3}$ and O K edges. The spectra show that in La_2CoO_4, the superexchange between neighboring Co^{2+} HS states is responsible for the strong antiferromagnetism. With increasing hole doping, the superexchange interactions between Co^{2+} HS ions are rapidly reduced by interlaced nonmagnetic Co^{3+} LS. For $La_{1.5}Ca_{0.5}CoO_4$, the low Néel temperature of the samples together with the 50% Co^{2+} HS and 50% Co^{3+} LS configuration suggests a checkerboard arrangement of these ions. The spin blockade resulting from this arrangement naturally explains the high resistivity of $La_{1.5}Ca_{0.5}CoO_4$. Upon further doping, Co^{2+} HS ions are replaced by Co^{3+} HS, and for $LaCaCoO_4$ a mixture of Co^{3+} LS and Co^{3+} HS occurs. Superexchange via configuration fluctuation processes between these two species seems to induce long-range ferromagnetism, while the superexchange between adjacent Co^{3+} HS neighbors may lead to a competing antiferromagnetic exchange. For a doping content beyond $x = 1$, Co^{4+} HS is introduced to the system at the expense of Co^{3+} LS, and a t_{2g} double exchange between Co^{3+} HS and Co^{4+} HS is established, which further enhances ferromagnetic interactions and reduces resistivity. No indications for a Co^{3+} IS state are found throughout the $La_{2-x}Ca_xCoO_4$ doping series.

DOI: 10.1103/PhysRevB.84.014436 PACS number(s): 78.70.Dm, 71.20.−b, 75.30.Et, 75.47.Lx

I. INTRODUCTION

For many transition-metal oxides, the intricate interplay between charge, spin (up or down), orbital, and lattice degrees of freedom leads to interesting and unusual electronic and magnetic phenomena such as high-temperature superconductivity, colossal magnetoresistance, and complex magnetic orbital ordering. In the case of the cobaltates, an additional intriguing aspect is found—the *spin state* degree of freedom. Depending on the delicate balance between the crystal-field splitting Δ_{CF}, i.e., the energetic splitting between t_{2g} and e_g orbitals, and the exchange interaction J_{ex} associated with Hund's rule coupling, a Co^{3+} ion in a cubic O_h symmetry can occur in different spin states: a low-spin state (LS, $t_{2g}^6e_g^0$, $S = 0$) is stabilized for a strong crystal field, while a high-spin state (HS, $t_{2g}^4e_g^2$, $S = 2$) is found for a weak crystal-field splitting. Since the energy difference between these two ground states and the excited intermediate spin state (IS, $t_{2g}^5e_g^1$, $S = 1$) is so small that the latter may be thermally activated, the IS has also been discussed as a further possible ground state in the cobaltates.[1–10] A Co^{3+} IS ground state may be stabilized either by the gain of kinetic energy induced by a half-filled broad e_g conduction band or by a strong Jahn-Teller distortion. Yet despite the fact that no consensus has been reached so far, many investigations show that the IS configuration is energetically not favored for the tilted but essentially regular CoO_6 octahedron in $LaCoO_3$.[11–18] A more promising candidate for an IS state might be the single-layered $La_{2-x}Ca_xCoO_4$ compound: For this system, the K_2NiF_4 structure with the tetragonal space group $I4/mmm$ found for the doping range $0.3 \lesssim x \lesssim 0.8$ (and the orthorhombic space group $Bmab$ otherwise) leads to a considerable elongation of the octahedron and, consequently, to a notable splitting of the e_g states, which is a prerequisite for an IS state.[19–23]

The parent compound La_2CoO_4 is an antiferromagnetic insulator with a Néel temperature, T_N, of 275 K,[24–26] and the Co^{2+} ion is in an HS ($t_{2g}^5e_g^2$, $S = 3/2$) configuration. Partial replacement of La^{3+} by Ca^{2+} or Sr^{2+} introduces holes to the system and changes the corresponding Co valency from +2 to +3. Concomitant with hole-doping, the substitution leads to a rapid suppression of the antiferromagnetic ground state, and a checkerboard arrangement of Co^{2+} HS and Co^{3+} LS states is observed for the related $La_{1.5}Sr_{0.5}CoO_4$ system.[27,28] The spin blockade resulting from this configuration explains both the high charge-ordering temperature ($T_{CO} \approx 750$ K) and the low spin-ordering temperature ($T_{SO} \lesssim 30$ K).[27,29,30] Upon further hole doping, the resistivity is strongly reduced, and for $LaSrCoO_4$ (which contains only Co^{3+}), the magnitude of the resistivity is of the same order as that of $LaCoO_3$.[31,32] Nevertheless, no indication for mobile charge carriers is found. Due to the concurrent decrease of the effective moment per Co site, μ_{eff}(Co), and the Weiss temperature, Θ, it was suggested that some induced ferromagnetic interaction competes with the original superexchange antiferromagnetism.[31] The Co^{4+} doping for samples with a doping content $x > 1$ establishes ferromagnetism and leads to a significant reduction of the resistivity due to the presence of mobile charge carriers.[32] Similarly to Co^{3+}, the Co^{4+} ion can in principle have an HS ($t_{2g}^3e_g^2$, $S = 5/2$), an LS ($t_{2g}^5e_g^0$, $S = 1/2$), or an IS ($t_{2g}^4e_g^1$, $S = 3/2$) configuration. To explain the doping-dependent transport, magnetic, and structural characteristics of $La_{2-x}Sr_xCoO_4$ and $La_{2-x}Ca_xCoO_4$, several scenarios for the Co^{3+} spin state have been suggested for the doping series, ranging from Co^{3+} LS (Refs. 27 and 28) to Co^{3+} IS states (Refs. 29 and 30) and finally to HS/IS transitions[31] and HS/IS mixtures.[22,23]

To shed more light on the doping-dependent orbital and spin states of the Co ion in the single-layered cobaltates, we have investigated the $La_{2-x}Ca_xCoO_4$ system ($x = 0$, 0.5, 1, and 1.5) with temperature-dependent near-edge x-ray absorption fine structure (NEXAFS) at the Co $L_{2,3}$ and O K edges. Utilizing multiplet simulations, the configuration of the corresponding spin, orbital, and valence states is determined for the investigated doping contents. To explain the doping-dependent changes of the absorption spectra and of the magnetic properties of the samples, a microscopic picture of the relevant magnetic and electronic interactions is developed.

The paper is organized as follows: Section II covers sample preparation and data collection. In Secs. III A and III B, we will expound the features of the Co $L_{2,3}$ and O K NEXAFS studies. Section III C discusses the implications of the NEXAFS results in view of a microscopic picture of the spin-state structure and the exchange mechanism. Finally, in Sec. III D the temperature dependence of the spin states is examined. The results are summarized in Sec. IV.

II. EXPERIMENTAL

Polycrystalline $La_{2-x}Ca_xCoO_4$ samples with $x = 0$, 0.5, 1, and 1.5 were prepared by standard solid-state reaction using La_2O_3, $CaCO_3$, and CoO powders with a purity $\geqslant$ 99.9% as starting materials. First, the powders were mixed in stoichiometric composition and calcinated at 950 °C for 24 h. Before sintering, the powders were milled in a ball-mill for 30 min. The first sintering step was carried out at 1150 °C for 40 h under ambient conditions. After the first sintering step, the powders were ground again and pressed to pellets with a diameter of 12 mm. Since the melting temperature of the composition decreases with increasing Ca content, the sintering temperature was also decreased from 1350 °C to 1300, 1200, and 1150 °C for $x = 0$, 0.5, 1, and 1.5, respectively. The second sintering step was carried out for 40 h under ambient conditions for $x \geqslant 0.5$. Undoped La_2CoO_4 samples were sintered in vacuum at 10^{-4} mbar to achieve complete reduction of cobalt to Co^{2+}. The samples were characterized by x-ray diffraction (XRD) and by superconducting quantum interference device (SQUID) magnetometry. For the latter, the effective magnetic moment was deduced from the inverse of the susceptibility measured in the temperature range $200 < T < 300$ K.[20] The lattice parameters, the space group (SG), the Néel temperature T_N, and the Curie temperature T_C for $La_{2-x}Ca_xCoO_4$ ($x = 0.0$, 0.5, 1.0, and 1.5) samples are given in Table I. The XRD and magnetometry results are consistent with the structural formula of the samples. As a representative example, the Rietveld refinement on the room-temperature x-ray diffraction pattern of $La_{1.5}Ca_{0.5}CoO_4$ (after Ref. 20) is shown in Fig. 1. The powder patterns were measured in the 2Θ range between 10° and 95°, and refined employing the FULLPROF program package. Despite two very small unindexed reflections around $2\Theta = 29.9°$ and 39.5° (with an intensity $I < 5\%$ compared to the 113 reflection of $La_{1.5}Ca_{0.5}CoO_4$), contributions from secondary phases can be excluded. The reduction from the tetragonal $I4/mmm$ to the orthorhombic $Bmab$ symmetry for samples with $x \neq 0.5$ might be induced by the tilting of the CoO_6 octahedra due to the decrease of the averaged ionic radius of the (La, Ca) site produced by the Ca substitution. Alternatively, a small amount of oxygen deficiency (see NEXAFS valence analysis below) might be responsible for the tilting. In the latter case, however, neither XRD nor magnetometry is sufficiently sensitive to determine such small deviations from the expected stoichiometric oxygen content.

TABLE I. Lattice parameters, space group (SG), Néel temperature T_N, and Curie temperature T_C for $La_{2-x}Ca_xCoO_4$ ($x = 0.0$, 0.5, 1.0, and 1.5). The pseudocubic in-plane lattice parameter [a for $I4/mmm$ and $(a+b)/(2\times\sqrt{2})$ for $Bmab$], the c lattice parameter, and as consequence also the volume of the unit cell strongly shrink upon Ca doping. Specimens with Ca contents of $x = 0.0$ and 0.5 are antiferromagnetic while those with $x = 1.0$ and 1.5 are ferromagnetic.

x	SG	a (Å)	b (Å)	c (Å)	T_N (K)	T_C (K)
0.0	$Bmab$	5.521(3)	5.486(3)	12.631(5)	275	
0.5	$I4/mmm$	3.819(2)		12.300(5)	8	
1.0	$Bmab$	5.429(3)	5.363(3)	12.101(5)		92
1.5	$Bmab$	5.393(3)	5.351(3)	11.964(5)		140

Temperature-dependent NEXAFS measurements were performed at the Institut für Festkörperphysik beamline WERA at the ANKA synchrotron light source (Karlsruhe, Germany). The spectra at the Co $L_{2,3}$ edge were taken in total electron yield (TEY) while the fluorescence yield (FY) was utilized for the O K edge. Directly before data collection, the samples were scraped in a preparation chamber with a base pressure around 2×10^{-9} mbar and immediately transferred in ultrahigh vacuum to the NEXAFS chamber with a base pressure of 1×10^{-10} mbar. All spectra were measured with linearly polarized light and in a normal-incidence geometry.

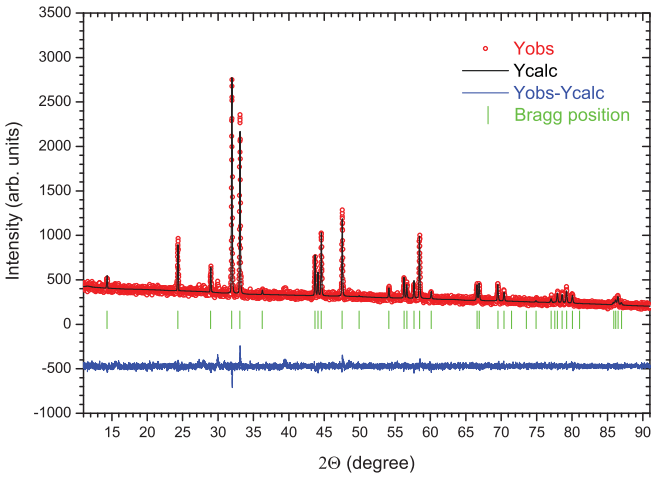

FIG. 1. (Color online) Rietveld refinement of the room-temperature x-ray diffraction pattern of $La_{1.5}Ca_{0.5}CoO_4$ (after Ref. 20), shown as a representative example for the series investigated. Measured data are shown as red dots, calculated data as a black curve, and the difference between measured and calculated data as a blue curve that is vertically offset from the zero line. All fundamental reflections can be indexed using space group $I4/mmm$. The expected Bragg positions are indicated as green tick marks. The strong background is due to Co fluorescence induced by the Cu $K\alpha_1$ radiation.

The energy resolution of the absorption spectra was set to 0.3 eV for the Co $L_{2,3}$ edge and to 0.15 eV for the O K edge. After correction for photon flux variations and for the background, the spectra were normalized at the edge jump. Saturation and self-absorption effects, usually unavoidable for FY data, were corrected with the method outlined in Refs. 33–37. Photon energy calibration was ensured by adjusting the Ni L_3 peak position measured on a NiO single crystal before and after each NEXAFS scan to the established peak position.[18]

III. RESULTS AND DISCUSSION

A. Co $L_{2,3}$ NEXAFS

The Co $L_{2,3}$ NEXAFS spectra of $La_{2-x}Ca_xCoO_4$ (x = 0, 0.5, 1, and 1.5) are displayed in Fig. 2.[38] Due to the strong charging effects observed for lower temperature, only the 300 K TEY data are depicted. The absorption spectra correspond in first order to transitions of the type Co $2p^6 3d^n \rightarrow$ Co $2p^5 3d^{n+1}$ (n = 5, 6, and 7 for Co^{4+}, Co^{3+}, and Co^{2+}, respectively). They consist of two manifolds of multiplets situated around 780 eV (L_3) and 795 eV (L_2) and separated by the spin-orbit splitting of the Co $2p$ level. The labeling of the spectral features is given in Figs. 2 and 3. For the Co L_3 edge of La_2CoO_4, the first feature is observed at 777.4 eV (P1) followed by a strong peak at 778.7 eV (P2). From the changes in the slope, a further feature around 780.2 eV (P3) can already be inferred for this sample from the measured data. A small shoulder (P4) is found around 781.7 eV. At the L_2 edge, peak P5 is found around 794 eV with a small shoulder both on the low-energy and high-energy side. Upon hole doping, i.e., for $La_{1.5}Ca_{0.5}CoO_4$, the spectral weight of P1 and P2 is reduced and features P3 and P4 strongly increase. At the L_2 edge, a double-peak structure is found with a strong peak P5 and a considerably smaller feature P6. For $LaCaCoO_4$, the spectral weight of features P1 and P2 diminishes while P3 and P4 grow significantly. Furthermore, the ratio between P5 and P6 changes: peak P6 clearly increases at the expense of P5. Nevertheless, P5 remains the dominant feature. Finally, when going from $LaCaCoO_4$ to $La_{0.5}Ca_{1.5}CoO_4$, feature P2 increases, P3 remains essentially constant, and P4 flattens. Moreover, the ratio between P5 and P6 is further reduced.

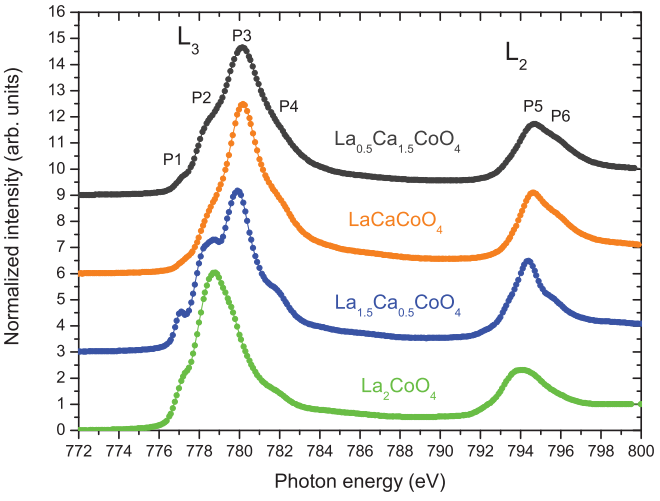

FIG. 2. (Color online) Comparison of the Co $L_{2,3}$ NEXAFS spectra of La_2CoO_4, $La_{1.5}Ca_{0.5}CoO_4$, $LaCaCoO_4$, and $La_{0.5}Ca_{1.5}CoO_4$ taken at 300 K. The spectral shape of both edges strongly changes upon doping. For clarity, the spectra are vertically offset.

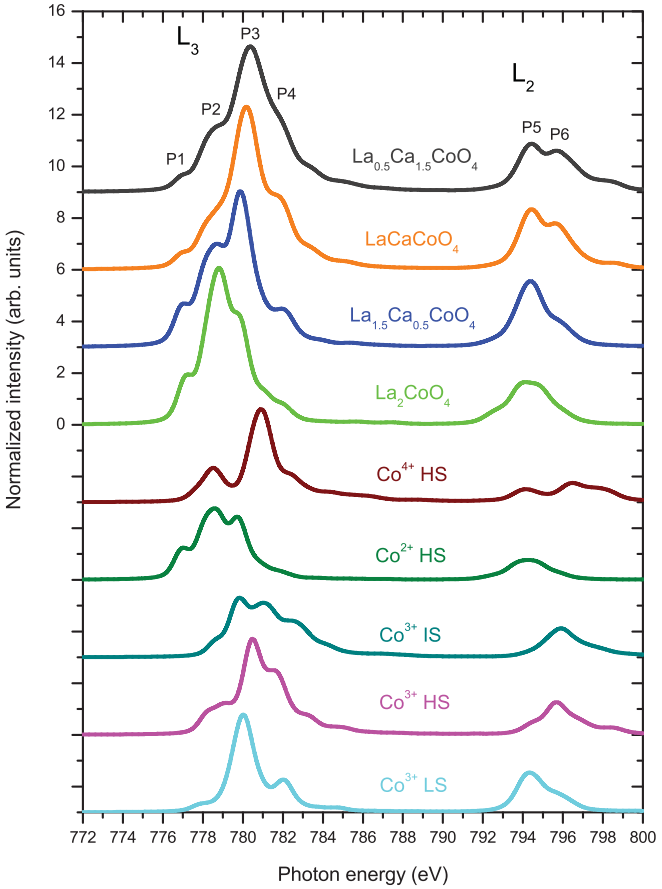

FIG. 3. (Color online) Co $2p$ XAS multiplet calculations of Co^{3+} LS, Co^{3+} HS, Co^{3+} IS, Co^{2+} HS, and Co^{4+} HS. In addition, the simulated spectra of La_2CoO_4, $La_{1.5}Ca_{0.5}CoO_4$, $LaCaCoO_4$, and $La_{0.5}Ca_{1.5}CoO_4$ are also displayed. For clarity, the spectra for the different configurations are vertically offset. The simulated spectra are scaled to their corresponding experimental data in Fig. 2.

The spectra can be qualitatively analyzed in more detail using atomic-multiplet plus crystal-field calculations. The code developed by Thole[39–41] and maintained and further developed by de Groot[42–45] was used to calculate spectra for different values of the crystal-field splitting Δ_{CF} and of the charge-transfer energy Δ_c and by taking the (Hund's rule) exchange interaction into account. Charge-transfer effects were included for Co^{3+} by admixing transitions of the type $2p^6\ 3d^7\underline{L} \rightarrow 2p^5\ 3d^8\underline{L}$, where $\underline{L}$ denotes a hole in the oxygen ligand. Correspondingly, $2p^6\ 3d^8\underline{L} \rightarrow 2p^5\ 3d^9\underline{L}$ and $2p^6\ 3d^6\underline{L} \rightarrow 2p^5\ 3d^7\underline{L}$ transitions were admixed for Co^{2+} and Co^{4+}, respectively. The Slater integrals were renormalized to 80% of their Hartree-Fock values to approximately account for intra-atomic configuration interactions. To compare the calculated data with the experiment, a Lorentzian broadening with σ = 0.2 eV (σ = 0.3 eV) and a Gaussian broadening with σ = 0.3 eV were applied to the L_3 (L_2) edge to approximately

account for lifetime, phononic, and resolution effects. All multiplet calculations were performed for a D_{4h} symmetry of the octahedron. The spectra obtained in this way for the a_1, a_2, and the c direction were averaged to account for the polycrystalline nature of the samples. Figure 3 shows the calculated Co $2p$ XAS spectra of Co^{3+} LS, Co^{3+} HS, Co^{3+} IS, Co^{2+} HS, and Co^{4+} HS.[46] The calculated spectra are similar to previous multiplet calculations.[14,15,18,27,47,48] The small variance between the present and our previous spectra[18] is due to the fact that the current calculations were performed taking account of the tetragonal D_{4h} distortion of the octahedron in $La_{2-x}Ca_xCoO_4$, while for the calculations in Ref. 18, the cubic O_h symmetry of the regular octahedron in $La_{1-x}A_xCoO_3$ (where A denotes Sr or Ce) was used. In addition, the simulated spectra of La_2CoO_4, $La_{1.5}Ca_{0.5}CoO_4$, $LaCaCoO_4$, and $La_{0.5}Ca_{1.5}CoO_4$ are also depicted. The simulated spectra are obtained for appropriate linear combinations of the calculated single-configuration spectra. The shape of the simulated spectra strongly depends on the crystal field, charge transfer, spin-orbit coupling, intra-atomic configuration interactions, energetic position, and other parameters. All parameters were varied until a reasonable agreement with the experimental data in Fig. 2 was achieved. As starting parameters for the (relative) concentration of Co^{2+}, Co^{3+}, and Co^{4+} valence states, the values expected from the structural formula were used. The approximate distribution of valence and spin states finally derived from the multiplet simulations for La_2CoO_4, $La_{1.5}Ca_{0.5}CoO_4$, $LaCaCoO_4$, and $La_{0.5}Ca_{1.5}CoO_4$ is summarized in Table II. For reference, the parameters used for the calculated single-configuration spectra are given in Ref. 49. For a discussion of the valence and spin state of the Co ions, the simulations depicted in Fig. 3 reproduce fairly well all major features of the experimental results at both the L_3 and the L_2 edges in Fig. 2. Such a close resemblance between the simulated and measured spectra is possible only if the calculated valence and spin states are very close to the experimental situation in the corresponding samples.

The simulations in Fig. 3 show that the spectral shape of the La_2CoO_4 sample in Fig. 2 is correctly described by high-spin Co^{2+}.[50] In addition, the simulations indicate that the samples with a doping content $x > 0$ contain ≈20% more Co^{2+} than expected from the XRD and magnetometry data. This systematic deviation from stoichiometry suggests that *all* investigated samples (including La_2CoO_4) are slightly oxygen-deficient. From the simulations, the deviation from stoichiometric oxygen content is estimated to be ≈2%–3%.[51]

For $La_{1.5}Ca_{0.5}CoO_4$, the multiplet calculations illustrate that the spectral shape is a mixture of Co^{2+} HS and Co^{3+} LS (see also Table II). After elimination of the oxygen-deficiency-induced Co^{2+} contribution, we obtain a 50% Co^{2+} HS/50% Co^{3+} LS configuration for $La_{1.5}Ca_{0.5}CoO_4$. This clearly shows that similar to $La_{1.5}Sr_{0.5}CoO_4$, a checkerboard arrangement of Co^{2+} HS and Co^{3+} LS is highly probable for $x = 0.5$ in the Ca-doped system. Such an arrangement leads to a low antiferromagnetic spin-ordering temperature and, hence, is consistent with the low T_N value of $La_{1.5}Ca_{0.5}CoO_4$ in Table I.

For $LaCaCoO_4$, a mixture of 55% Co^{3+} LS/45% Co^{3+} HS can be inferred from the simulations. Thus, upon hole doping, Co^{2+} HS is for the most part replaced by Co^{3+} HS. As already pointed out for epitaxially strained $LaCoO_3$ films,[18] a mixture of Co^{3+} LS and Co^{3+} HS states can lead to ferromagnetic superexchange via configuration fluctuation processes. It should be mentioned that the number of Co^{3+} HS ions is even higher in the polycrystalline $LaCaCoO_4$ samples investigated here than in the epitaxial $LaCoO_3$ films of Ref. 18. This difference, together with the changes of the pseudocubic in-plane lattice parameter from 3.801 Å for $LaCaO_3$ to 3.816 Å for $LaCaCoO_4$, might be attributed to a reduced chemical pressure for the $La_{2-x}Ca_xCoO_4$ system. The increase of the Co^{3+} HS fraction observed for the single-layered system is an important finding, and we will discuss this item in more detail in the context of a microscopic picture of the magnetic exchange mechanism below.

Finally, for $La_{0.5}Ca_{1.5}CoO_4$, a 20% Co^{4+} HS, 35% Co^{3+} LS, and 45% Co^{3+} HS configuration is obtained from the multiplet simulations. This shows that the "effective" doping content of the nominally $La_{0.5}Ca_{1.5}CoO_4$ sample is smaller than expected and is around $x = 1.2$. The reduced "effective" doping content, however, is most probably caused by oxygen deficiency in the surface layers mainly probed by TEY, since no indications for a reduced doping content are observed in the bulk-sensitive magnetometry data.[52] Consequently, we will continue to refer to this sample as $La_{0.5}Ca_{1.5}CoO_4$ throughout the remainder of the paper. Moreover, the multiplet simulations suggest that Co^{3+} LS is partially substituted by Co^{4+} HS when going from $LaCaCoO_4$ to $La_{0.5}Ca_{1.5}CoO_4$ while the number of Co^{3+} HS states remains constant. The doping-dependent changes of the valence and spin states (after elimination of the oxygen-deficiency-induced Co^{2+}) are summarized in Table II.

It seems also worthwhile to explicitly mention that the measured data of La_2CoO_4, $La_{1.5}Ca_{0.5}CoO_4$, $LaCaCoO_4$, and $La_{0.5}Ca_{1.5}CoO_4$ can be simulated quite well without taking a Co^{3+} IS state into account. In principle, already the spectral shape of the simulated Co^{3+} IS state with its broad multiplet structures at the $L_{2,3}$ edges (see Fig. 3) clearly demonstrates that it cannot be a significant species in the system under study here. On the basis of our multiplet calculations, a Co^{3+} IS state is stabilized for the tetragonal (orthorhombic) symmetry of the K_2NiF_4 structure only for a splitting of the e_g doublet ($x^2 - y^2$, $3z^2 - r^2$) beyond ≈2 eV. While a large structural distortion of the CoO_6 octahedron leads indeed to a considerable splitting of the e_g states (typically of ≈0.7 eV as derived for $La_{2-x}Ca_xCoO_4$ from our multiplet calculations), it apparently falls far short of the ≈2 eV required to stabilize the

TABLE II. Approximate distribution of valence and spin states derived from the multiplet simulations for La_2CoO_4, $La_{1.5}Ca_{0.5}CoO_4$, $LaCaCoO_4$, and $La_{0.5}Ca_{1.5}CoO_4$ after elimination of the oxygen-deficiency-induced Co^{2+} contribution. The estimated uncertainty of each value is ≈2%–3%.

	Co^{2+} HS	Co^{3+} LS	Co^{3+} HS	Co^{4+} HS
La_2CoO_4	100%			
$La_{1.5}Ca_{0.5}CoO_4$	50%	50%		
$LaCaCoO_4$		55%	45%	
$La_{0.5}Ca_{1.5}CoO_4$		35%	45%	20%

IS state as a ground state in our calculations. This interpretation is consistent with local-spin-density approximation plus Hubbard U calculations (LSDA + U) where also spin-orbit coupling and multiplet effects were included.[53–56] A further prerequisite for a stable Co^{3+} IS configuration is that the $3z^2 - r^2$ orbital lies energetically slightly above the xz, yz states and that the xy orbital is lowest in energy. Moreover, the probability to find a hole at the O site, described for Co^{3+} by the $2p^6 3d^7 \underline{L}$ configuration, increases from ≈13% for an HS state to ≈22% for an LS state and finally to ≈50% for the IS state. Corresponding to our calculations, similar arguments hold for the corresponding Co^{4+} configurations. Thus, an IS state is stabilized only if a very strong crystal field ($\Delta_{CF} \gtrapprox 2.4$ eV), an unusually strong distortion of the CoO_6 octahedron ($\Delta_{JT} \gtrapprox 2.0$ eV), and a significant hybridization between the Co ion and its O neighbors are present, as suggested in Ref. 1.

B. O *K* NEXAFS

In Fig. 4, the O K NEXAFS spectra of La_2CoO_4, $La_{1.5}Ca_{0.5}CoO_4$, $LaCaCoO_4$, and $La_{0.5}Ca_{1.5}CoO_4$ taken at 40 K are compared between 526 and 534 eV.[38] In this energy range, the spectra reflect the unoccupied O $2p$ states hybridized with Co $3d$ e_g and t_{2g} orbitals. The low-temperature O K edge data were taken in the FY mode to avoid charging problems that otherwise could occur for TEY at low temperature.[27] For La_2CoO_4, only a small peak appears in the relevant energy range below 531.5 eV. Corresponding to the $t_{2g}^5 e_g^2$ configuration of the Co^{2+} HS state, the small spectral weight of this peak reflects the small number of holes in e_g states and an even smaller number in t_{2g} states. Furthermore, the hybridization between the Co $3d$ and the O $2p$ orbitals is weak for Co^{2+}, as indicated by the probability of ≈13% for the $2p^6 3d^8 \underline{L}$ configuration (determined from the multiplet calculations), and, thus, the intrinsically doped holes reside predominantly on the Co ion.

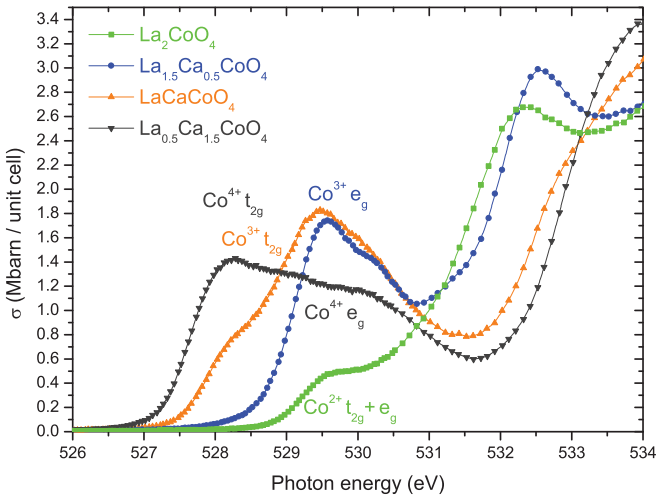

FIG. 4. (Color online) O K NEXAFS spectra of La_2CoO_4, $La_{1.5}Ca_{0.5}CoO_4$, $LaCaCoO_4$, and $La_{0.5}Ca_{1.5}CoO_4$ taken at 40 K. The spectral weight for O $2p$ states hybridized with e_g and t_{2g} levels is strongly doping-dependent. Rough estimates for the valence-dependent t_{2g} and e_g regions are indicated in the figure.

For $La_{1.5}Ca_{0.5}CoO_4$, a strong double-peak structure centered around 530 eV is found in the absorption spectra. Despite a certain energetic overlap between the t_{2g} spin-down region and the e_g spin-up area caused by the exchange splitting,[57] it has been established by temperature-dependent NEXAFS that the Co^{3+} e_g spin-up states are situated around 530 eV while the Co^{3+} t_{2g} spin-down states are found below ≈529 eV.[15,18,47] Therefore, the feature at 530 eV corresponds to a large number of unoccupied states in the area dominated by Co^{3+} e_g states. The intensity in the predominantly t_{2g} area (below 529 eV), on the other hand, is very low. This spectral-weight distribution is consistent with the 50% Co^{2+} HS/50% Co^{3+} LS ratio derived from the Co $L_{2,3}$ edge, where for the 50% Co^{3+} LS states ($t_{2g}^6 e_g^0$ configuration) both e_g levels are empty and the t_{2g} orbitals are completely filled. Furthermore, as can be inferred from the La_2CoO_4 spectrum, the 50% Co^{2+} HS ions ($t_{2g}^5 e_g^2$ configuration) in $La_{1.5}Ca_{0.5}CoO_4$ do not significantly contribute to the energy range below 531 eV. The current data for $La_{1.5}Ca_{0.5}CoO_4$ are very similar to the results found for the checkerboard arrangement of Co^{2+} HS and Co^{3+} LS in $La_{1.5}Sr_{0.5}CoO_4$.[27] Using LDA + U calculations, it was also shown in Ref. 27 that the first peak of the double-peak structure at 529.5 eV can be ascribed to O $2p_z$–Co $3d_{z^2-r^2}$ hybrids, while the second one ≈0.7 eV higher in energy is attributed to O $2p_{x,y}$–Co $3d_{x^2-y^2}$ hybrids.

When going to $LaCaCoO_4$ (which contains only Co^{3+}), the spectral weight of the e_g range remains almost unaffected by the doping while the spectral weight in the t_{2g} range increases. More specifically, the doped holes are predominantly found in the t_{2g} orbitals, i.e., the number of Co^{3+} HS clearly increases upon hole doping while the number of Co^{3+} LS remains approximately unchanged. This distribution of the spectral weight, however, is expected for the mixture of 55% Co^{3+} LS ($t_{2g}^6 e_g^0$ configuration) and 45% Co^{3+} HS ($t_{2g}^4 e_g^2$ configuration) determined for $LaCaCoO_4$ from the multiplet simulations. In other words, the observed spectral changes strongly support the picture obtained from the Co $L_{2,3}$ edges that Co^{2+} HS ($t_{2g}^5 e_g^2$ configuration) is substituted by Co^{3+} HS. Furthermore, a Co^{3+} IS state ($t_{2g}^5 e_g^1$ configuration) can be ruled out for $LaCaCoO_4$ from the O K NEXAFS spectra, too:[58] If Co^{3+} IS states were indeed introduced to the system upon Ca doping instead of Co^{3+} HS (instead of Co^{3+} LS), the e_g spectral weight, i.e., the number of unoccupied Co^{3+} e_g states, would have increased (would have decreased) when going from $La_{1.5}Ca_{0.5}CoO_4$ to $LaCaCoO_4$ which is, however, not the case. Despite a small overlap between the t_{2g} and the e_g region (see discussion above), the crystal-field splitting might be roughly estimated from the Co^{3+} t_{2g} and Co^{3+} e_g peak positions to be ≈1.0–1.4 eV.

For $La_{0.5}Ca_{1.5}CoO_4$, i.e., for a doping content $x > 1$, the absorption intensity at 530 eV is significantly reduced while the spectral weight around 528 eV is considerably increased. To analyze this finding, we take a closer look at the distribution of valence and spin states derived from the Co $L_{2,3}$ edges and from the multiplet simulations (see also Table II): When going from $LaCaCoO_4$ to $La_{0.5}Ca_{1.5}CoO_4$, the 45% Co^{3+} HS remain unaffected by the doping while ≈ 20% Co^{3+} LS are replaced by Co^{4+} HS ($t_{2g}^3 e_g^2$ configuration). Hence the decrease of spectral weight around 530 eV can be directly attributed to the reduced

number of Co^{3+} LS states and, as a consequence of the fact that the number of Co^{3+} HS remains unchanged, the increase of spectral weight around 528 eV is unequivocally correlated with the Co^{4+} t_{2g} spin-down states. Rough estimates for the energetic position of the O $2p$ orbitals hybridized with Co^{4+} e_g spin-up states can be inferred using the multiplet calculations from which they are expected to reside ≈1.5–2.0 eV above the Co^{4+} t_{2g} spin-down states. Taken together, the O K absorption data are fully consistent with and corroborate the spin and orbital configurations found at the Co $L_{2,3}$ edge.

C. Microscopic picture and exchange mechanism

To discuss the magnetic exchange mechanism between the valence-dependent spin states in terms of a microscopic picture, a sketch showing the relevant local hopping processes for

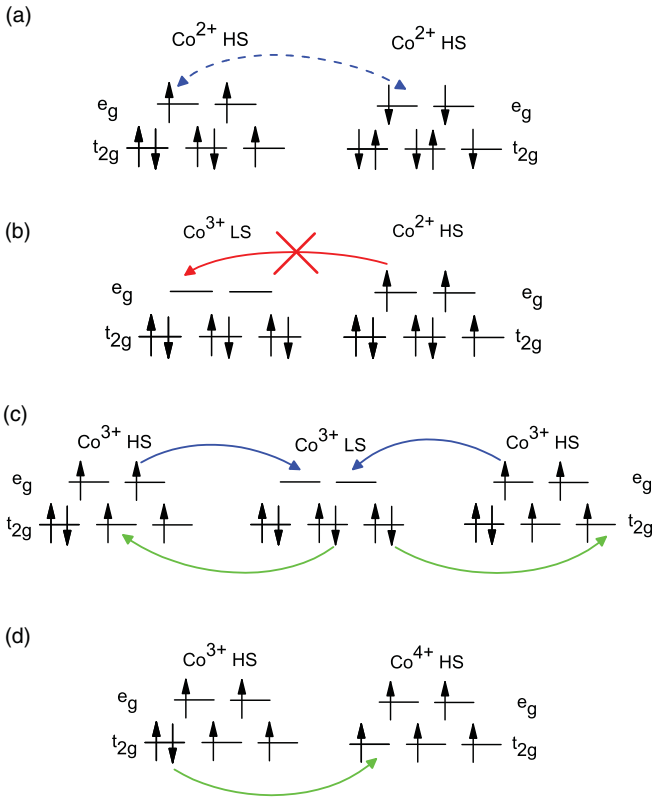

FIG. 5. (Color online) Scheme showing the orbital occupation and the relevant hopping process for $La_{2-x}Ca_xCoO_4$. (a) Virtual hopping processes between the two Co^{2+} HS neighbors in La_2CoO_4 induce antiferromagnetic ordering. As a representative, only the virtual hopping of an e_g electron is shown. In principle, all electrons in half-filled orbitals can perform such processes. (b) For $La_{1.5}Ca_{0.5}CoO_4$, the spin blockade inhibits the transfer of an electron from the Co^{2+} HS to the Co^{3+} LS site. (c) For $LaCaCoO_4$, correlated t_{2g} and e_g hopping processes between Co^{3+} LS and Co^{3+} HS neighbors lead to a ferromagnetic superexchange. Due to the correlated hopping of t_{2g} and e_g electrons, spin states are interchanged without a net transfer of charge. In the sketch, only the local t_{2g} and e_g hopping processes for the transformation of a Co^{3+} LS into a Co^{3+} HS ion are considered (Refs. 62 and 63). (d) For the t_{2g} double exchange in $La_{0.5}Ca_{1.5}CoO_4$, an electron moves from a Co^{3+} HS site to a Co^{4+} HS neighbor.

La_2CoO_4, $La_{1.5}Ca_{0.5}CoO_4$, $LaCaCoO_4$, and $La_{0.5}Ca_{1.5}CoO_4$ is presented in Fig. 5.[59] The situation for La_2CoO_4 is outlined in Fig. 5(a): Virtual hopping processes of electrons in half-filled orbitals lead to an antiferromagnetic ordering of the Co^{2+} HS neighbors and to a high Néel temperature ($T_N = 275$ K). For $La_{1.5}Ca_{0.5}CoO_4$ [Fig. 5(b)], the checkerboard arrangment of Co^{3+} LS and Co^{2+} HS ions nicely explains the highly insulating behavior of the samples despite a significant doping content: If one considers the hopping of an electron from a Co^{2+} HS ($S = 3/2$) site to its Co^{3+} LS ($S = 0$) neighbor, it is evident that the hopping process will produce a Co^{3+} IS ($S = 1$) and a Co^{2+} LS ($S = 1/2$) ion. Since such a change of the spin state costs a significant amount of energy, the hopping of charge carriers between these two types of Co ions is strongly inhibited.[27] This type of suppression of the conductivity is known as a spin blockade.[18,27,60] Furthermore, the spin blockade explains the strong lowering of T_N to about 8 K (see Table I) when going from La_2CoO_4 to $La_{1.5}Ca_{0.5}CoO_4$ due to the reduced number of paths with strong antiferromagnetic superexchange interactions between Co^{2+} HS neighbors. At first glance, spin ordering should even be completely suppressed for an ideal Co^{2+} HS/Co^{3+} LS checkerboard arrangement. However, a preferred spin orientation caused by the quasi-two-dimensional K_2NiF_4 structure may induce a weak residual spin ordering between next-nearest neighbors. Alternatively, the T_N value of 8 K may be due to small variations in the doping content or small defects in the ideal checkerboard arrangement with residual antiferromagnetic clusters of Co^{2+} HS neighbors.

For $LaCaCoO_4$, configuration-fluctuation processes [see Fig. 5(c)] between Co^{3+} HS and Co^{3+} LS neighbors can induce ferromagnetic interactions similar to the situation found for epitaxially strained $LaCoO_3$ films.[18] In contrast to the $LaCoO_3$ films, however, where ≈35% Co^{3+} HS states are introduced to the Co^{3+} LS matrix and (at least partially) arrange themselves with the LS species in a checkerboard-like manner,[18] the statistically distributed ≈45% Co^{3+} HS in $LaCaCoO_4$ may lead to two competing magnetic aspects: a ferromagnetic configuration-fluctuation interaction between Co^{3+} HS and Co^{3+} LS neighbors (mentioned above) and, due to the increased probability to also find adjacent Co^{3+} HS ions, an antiferromagnetic superexchange between Co^{3+} HS neighbors. In a microscopic picture, the latter exchange mechanism is similar to the one depicted in Fig. 5(a) for Co^{2+} HS. The coexistence of these two kinds of interactions explains very well the simultaneous appearance of ferro- and antiferromagnetic signatures in magnetometry experiments on $LaSrCoO_4$ (Ref. 31). The high Curie temperature ($T_C \approx 92$ K, see Table I) of $LaCaCoO_4$ and the fact that the ferromagnetism prevails over the antiferromagnetic exchange might be explained by percolative effects: Apparently, many of the clusters with the ferromagnetic Co^{3+} HS–Co^{3+} LS checkerboard arrangement are large enough to contribute to a long-range magnetic ordering, while the regions with adjacent Co^{3+} HS pairs seem to be mostly below the quasi-two-dimensional percolation threshold of the single-layered K_2NiF_4 structure and/or are rare compared to their ferromagnetic counterparts.

Finally, for $La_{0.5}Ca_{1.5}CoO_4$, the t_{2g} double exchange between Co^{3+} HS and Co^{4+} HS neighbors illustrated in Fig. 5(d) is consistent with the metallic and ferromagnetic behavior

found in Refs. 31 and 32 for a doping content $x > 1$ and nicely explains the strong increase in T_C from 92 to 140 K when going from $LaCaCoO_4$ to $La_{0.5}Ca_{1.5}CoO_4$ (see also Table I). Based on the present NEXAFS investigation, it cannot be excluded that, in addition to the t_{2g} Co^{3+} HS/Co^{4+} HS double exchange, electron transport or even band formation might also be possible for $La_{0.5}Ca_{1.5}CoO_4$ by e_g electron hopping between Co^{3+} HS/Co^{4+} HS sites and the remaining Co^{3+} LS ions. Such hopping processes could contribute to the conductivity and to the magnetic properties of the sample as well.

D. Temperature dependence

Finally, the temperature-dependent behavior of $La_{2-x}Ca_xCoO_4$ is discussed. This is an important issue since the spin state of the infinite-layer system $LaCoO_3$ changes with temperature: in bulk and polycrystalline $LaCoO_3$, Co^{3+} HS states are transformed to an LS configuration for $T \rightarrow 0$. The temperature-dependent O K NEXAFS spectra of $La_{2-x}Ca_xCoO_4$ ($x = 0.0$, 0.5, 1.0, 1.5) between 526 and 532 eV are compared in Fig. 6.[38] No temperature-dependent spectral changes are observed for La_2CoO_4, $La_{1.5}Ca_{0.5}CoO_4$, and $La_{0.5}Ca_{1.5}CoO_4$ between 40 and 300 K. The almost negligible broadening of the peaks found for these samples with increasing temperature can be attributed to phononic effects, and clearly shows that the spin-state structure is very stable in these systems. On the other hand, small changes in the distribution of the spectral weight and, thus, in the orbital occupation and in the spin-state structure occur for $LaCaCoO_4$: With decreasing temperature, the spectral weight in the Co^{3+} t_{2g} range is reduced while that in the Co^{3+} e_g area is slightly increased. According to the above discussion, this finding reflects the fact that for $LaCaCoO_4$, a certain amount of Co^{3+} goes from an HS to an LS state upon cooling. The observed changes are, however, quite small compared to bulk or polycrystalline $LaCoO_3$. It might be speculated that the comparatively high stability of the spin-state structure in $La_{2-x}Ca_xCoO_4$ is a consequence of the reduced dimensionality of the K_2NiF_4 structure and/or of the changes of the crystal-field splitting and the exchange interaction induced by the distorted CoO_6 octahedron and the modified Madelung potentials.

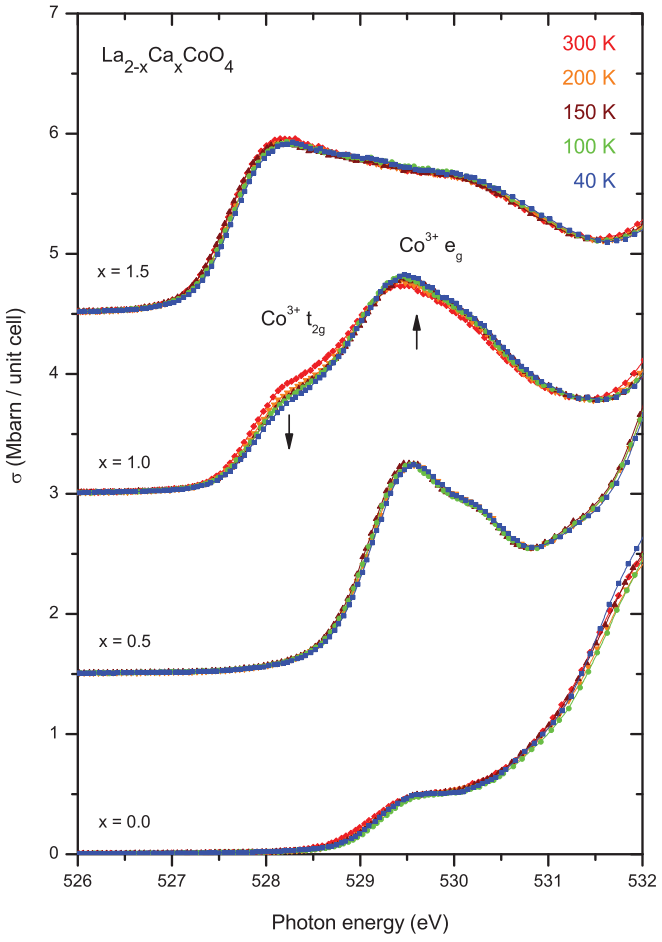

FIG. 6. (Color online) Temperature-dependent O K NEXAFS spectra of $La_{2-x}Ca_xCoO_4$ ($x = 0.0$, 0.5, 1.0, 1.5). No significant temperature dependence is found for La_2CoO_4, $La_{0.5}Ca_{1.5}CoO_4$, and $La_{1.5}Ca_{0.5}CoO_4$ while small changes in the spin-state structure occur for $LaCaCoO_4$.

IV. SUMMARY AND CONCLUSIONS

To shed more light on the spin and orbital states in single-layered $La_{2-x}Ca_xCoO_4$, NEXAFS measurements at the Co $L_{2,3}$ and O K edges were performed on samples with a doping content of $x = 0.0$, 0.5, 1.0, and 1.5. The data lead to the following picture for the orbital and spin-state structure: For La_2CoO_4, all Co^{2+} ions are in an HS states and the superexchange between these ions produces pronounced antiferromagnetism with a Néel temperature of 275 K. With increasing hole doping, Co^{3+} LS states are introduced to the system and replace Co^{2+} HS ions. The strong reduction of the Néel temperature to 8 K together with the 50% Co^{2+} HS/50% Co^{3+} LS ratio clearly support a checkerboard arrangement of these ions. A checkerboard arrangement not only diminishes the antiferromagnetic interactions between Co^{2+} HS ions but also explains the strongly insulating behavior of the sample: a spin blockade inhibits the transfer of an electron from the Co^{2+} HS to the Co^{3+} LS site.

Upon further doping, Co^{2+} HS ions are substituted by Co^{3+} HS, and for $LaCaCoO_4$ a mixture of 55% Co^{3+} LS and 45% Co^{3+} HS states occurs. This arrangement may lead to two competing magnetic effects: ferromagnetic configuration-fluctuation interactions between Co^{3+} HS and Co^{3+} LS neighbors, and antiferromagnetic superexchange between adjacent Co^{3+} HS neighbors as observed in Ref. 31 for $LaSrCoO_4$. The dominant ferromagnetic character of $LaCaCoO_4$ samples might be explained by the fact that either the domain size or the number of antiferromagnetic bonds is smaller than for their ferromagnetic counterparts.

Finally, for $La_{0.5}Ca_{1.5}CoO_4$ the multiplet simulations suggest that Co^{3+} LS is partially substituted by Co^{4+} HS for a doping content $x > 1$. The resulting t_{2g} double exchange between Co^{3+} HS and Co^{4+} HS neighbors induces metallic and ferromagnetic behavior and, thus, explains the strong increase in T_C from 92 to 140 K when going from $LaCaCoO_4$ to $La_{0.5}Ca_{1.5}CoO_4$.

In contrast to bulk $LaCoO_3$, no significant temperature-dependent spectral changes are observed for $La_{2-x}Ca_xCoO_4$,

implying that the spin-state structure is very robust in the quasi-two-dimensional single-layered system. Moreover, the NEXAFS studies at both Co L and O K edges did not give any indication for Co^{3+} intermediate spin states across the entire doping series. This finding also suggests that if a Co^{3+} intermediate spin configuration does not occur as a ground state for the considerably elongated CoO_6 octahedron of $La_{2-x}Ca_xCoO_4$, it is highly improbable that the intermediate spin state can exist for the essentially regular octahedron of $LaCoO_3$.

ACKNOWLEDGMENTS

We are indebted to B. Scheerer for his excellent technical support. We greatly appreciate stimulating discussions with F.M.F. de Groot about the intermediate spin state of cobalt ions. We gratefully acknowledge the Synchrotron Light Source ANKA Karlsruhe for the provision of beamtime. Part of this work was supported by the German Science Foundation (DFG) in the framework of the DFG Research Unit 960 "Quantum Phase Transitions."

*Corresponding author: michael.merz@kit.edu

[1] M. A. Korotin, S. Y. Ezhov, I. V. Solovyev, V. I. Anisimov, D. I. Khomskii, and G. A. Sawatzky, Phys. Rev. B **54**, 5309 (1996).

[2] T. Saitoh, T. Mizokawa, A. Fujimori, M. Abbate, Y. Takeda, and M. Takano, Phys. Rev. B **55**, 4257 (1997).

[3] C. Zobel, M. Kriener, D. Bruns, J. Baier, M. Grüninger, T. Lorenz, P. Reutler, and A. Revcolevschi, Phys. Rev. B **66**, 020402 (2002).

[4] P. Ravindran *et al.*, J. Appl. Phys. **91**, 291 (2002).

[5] T. Saitoh, T. Mizokawa, A. Fujimori, M. Abbate, Y. Takeda, and M. Takano, Phys. Rev. B **56**, 1290 (1997).

[6] S. Stølen, F. Grønvold, H. Brinks, T. Atake, and H. Mori, Phys. Rev. B **55**, 14103 (1997).

[7] G. Maris, Y. Ren, V. Volotchaev, C. Zobel, T. Lorenz, and T. T. M. Palstra, Phys. Rev. B **67**, 224423 (2003).

[8] G. Vankó, J.-P. Rueff, A. Mattila, Z. Németh, and A. Shukla, Phys. Rev. B **73**, 024424 (2006).

[9] J. M. Rondinelli and N. A. Spaldin, Phys. Rev. B **79**, 054409 (2009).

[10] K. Gupta and P. Mahadevan, Phys. Rev. B **79**, 020406 (2009).

[11] M. Zhuang, W. Zhang, and N. Ming, Phys. Rev. B **57**, 10705 (1998).

[12] S. Noguchi, S. Kawamata, K. Okuda, H. Nojiri, and M. Motokawa, Phys. Rev. B **66**, 094404 (2002).

[13] Z. Ropka and R. J. Radwanski, Phys. Rev. B **67**, 172401 (2003).

[14] M. W. Haverkort *et al.*, Phys. Rev. Lett. **97**, 176405 (2006).

[15] C. Pinta, D. Fuchs, M. Merz, M. Wissinger, E. Arac, H. v. Löhneysen, A. Samartsev, P. Nagel, and S. Schuppler, Phys. Rev. B **78**, 174402 (2008).

[16] N. Sundaram, Y. Jiang, I. E. Anderson, D. P. Belanger, C. H. Booth, F. Bridges, J. F. Mitchell, T. Proffen, and H. Zheng, Phys. Rev. Lett. **102**, 026401 (2009).

[17] R. Eder, Phys. Rev. B **81**, 035101 (2010).

[18] M. Merz, P. Nagel, C. Pinta, A. Samartsev, H. v. Löhneysen, M. Wissinger, S. Uebe, A. Assmann, D. Fuchs, and S. Schuppler, Phys. Rev. B **82**, 174416 (2010).

[19] X. Yang, L. Luo, and H. Zhong, Appl. Catal. A **272**, 299 (2004).

[20] D. Fuchs, M. Merz, R. Schneider, and H. v. Löhneysen, in *Oxide Nanoelectronics*, edited by H. Hwang, J. Levy, P. Makysymovych, G. Medeiros-Ribeiro, and R. Waser, MRS Symposium Proceedings No. 1292 (Materials Research Society, Pittsburgh, 2011).

[21] K. Horigane, T. Uchida, and J. Akimitsu, Physica B **378–380**, 334 (2006), Proceedings of the International Conference on Strongly Correlated Electron Systems—SCES 2005.

[22] K. Horigane, H. Hiraka, T. Uchida, K. Yamada, and J. Akimitsu, J. Phys. Soc. Jpn. **76**, 114715 (2007).

[23] K. Horigane, H. Nakao, Y. Kousaka, T. Murata, Y. Noda, Y. Murakami, and J. Akimitsu, J. Phys. Soc. Jpn. **77**, 044601 (2008).

[24] K. Yamada, M. Matsuda, Y. Endoh, B. Keimer, R. J. Birgeneau, S. Onodera, J. Mizusaki, T. Matsuura, and G. Shirane, Phys. Rev. B **39**, 2336 (1989).

[25] T. Matsuura, J. Tabuchi, J. Mizusaki, S. Yamauchi, and K. Fueki, J. Phys. Chem. Solids **49**, 1403 (1988).

[26] T. Matsuura, J. Tabuchi, J. Mizusaki, S. Yamauchi, and K. Fueki, J. Phys. Chem. Solids **49**, 1409 (1988).

[27] C. F. Chang *et al.*, Phys. Rev. Lett. **102**, 116401 (2009).

[28] N. Hollmann, M. W. Haverkort, M. Cwik, M. Benomar, M. Reuther, A. Tanaka, and T. Lorenz, New J. Phys. **10**, 023018 (2008).

[29] I. A. Zaliznyak, J. P. Hill, J. M. Tranquada, R. Erwin, and Y. Moritomo, Phys. Rev. Lett. **85**, 4353 (2000).

[30] I. A. Zaliznyak, J. M. Tranquada, R. Erwin, and Y. Moritomo, Phys. Rev. B **64**, 195117 (2001).

[31] Y. Moritomo, K. Higashi, K. Matsuda, and A. Nakamura, Phys. Rev. B **55**, R14725 (1997).

[32] A. V. Chichev *et al.*, Phys. Rev. B **74**, 134414 (2006).

[33] M. Merz *et al.*, Phys. Rev. B **55**, 9160 (1997).

[34] J. Goulon, C. Goulon-Ginet, R. Cortes and J. M. Dubois, J. Phys. (France) **43**, 539 (1982).

[35] D. M. Pease, D. L. Brewe, Z. Tan, J. I. Budnick, and C. D. C. Law, Phys. Lett. A **138**, 230 (1989).

[36] Z. Tan, J. I. Budnick, and S. M. Heald, Rev. Sci. Instrum. **60**, 1021 (1989).

[37] L. Tröger, D. Arvanitis, K. Baberschke, H. Michaelis, U. Grimm, and E. Zschech, Phys. Rev. B **46**, 3283 (1992).

[38] The error limits of each point are smaller than its symbol size.

[39] B. T. Thole and G. van der Laan, Europhys. Lett. **4**, 1083 (1987).

[40] B. T. Thole, G. van der Laan, and P. H. Butler, Chem. Phys. Lett. **149**, 295 (1988).

[41] G. van der Laan, B. T. Thole, G. A. Sawatzky, and M. Verdaguer, Phys. Rev. B **37**, 6587 (1988).

[42] F. M. F. de Groot, J. C. Fuggle, B. T. Thole, and G. A. Sawatzky, Phys. Rev. B **42**, 5459 (1990).

[43] F. M. F. de Groot, J. Electron Spectrosc. Relat. Phenom. **62**, 111 (1993).

[44] F. M. F. de Groot, Coord. Chem. Rev. **249**, 31 (2005).

[45] E. Stavitski and F. M. de Groot, Micron **41**, 687 (2010).

[46] In addition, multiplet calculations were also performed for Co^{2+} LS, Co^{4+} LS, and Co^{4+} IS configurations. Since they are, however, of no relevance for the simulation of the La_2CoO_4, $La_{1.5}Ca_{0.5}CoO_4$, $LaCaCoO_4$, and $La_{0.5}Ca_{1.5}CoO_4$ data, the spectra are omitted in Fig. 3.

[47]M. Abbate, J. C. Fuggle, A. Fujimori, L. H. Tjeng, C. T. Chen, R. Potze, G. A. Sawatzky, H. Eisaki, and S. Uchida, Phys. Rev. B **47**, 16124 (1993).

[48]Z. Hu *et al.*, J. Alloys Compd. **343**, 5 (2002).

[49]Multiplet parameters (in eV). Co^{2+} HS: 10 Dq = 0.8, Δ_c= 4.5, Δ_{e_g} = 0.7; Co^{3+} LS: 10 Dq = 1.9, Δ_c= 4.5, Δ_{e_g} = 0.7; Co^{3+} HS: 10 Dq = 1.2, Δ_c = 4.5, Δ_{e_g} = 0.7; Co^{3+} IS: 10 Dq = 2.6, Δ_c = −1.0, Δ_{e_g} = 2.38, $\Delta_{t_{2g}}$ = −0.14; Co^{4+} HS: 10 Dq = 2.0, Δ_c = 3.5, Δ_{e_g} = 0.6; for all spin and valence states, U_{dd}, U_{pd}, T_{e_g}, and $T_{t_{2g}}$ were set to 5.0, 6.0, 2.0, and 1.0, respectively. The Slater integrals were renormalized to 80% of their Hartree-Fock values.

[50]Please note that the Co^{2+} spectrum depicted in Fig. 3 is the one used for the simulation of the $La_{1.5}Ca_{0.5}CoO_4$ data. Small changes of the crystal-field parameters lead to the simulated La_2CoO_4 spectrum.

[51]It might be speculated that the oxygen deficiency and the corresponding additional Co^{2+} observed for all investigated samples are confined to the surface layer, which is to a large extent probed in TEY measurements. Due the fact, however, that (independent of its origin) the additional Co^{2+} fraction is eliminated in the evaluation process anyway, the interpretation given below for the spin states and the corresponding exchange mechanism remains unaffected.

[52]In this scenario, the oxygen deficiency in the surface layers is supposed to reduce the valence of some Co ions from +4 to +3.

[53]M. W. Haverkort, Ph.D. thesis, Universität zu Köln (2005).

[54]H. Wu and T. Burnus, Phys. Rev. B **80**, 081105 (2009).

[55]H. Wu, Phys. Rev. B **81**, 115127 (2010).

[56]T. Jia, H. Wu, G. Zhang, X. Zhang, Y. Guo, Z. Zeng, and H. Q. Lin, Phys. Rev. B **82**, 205107 (2010).

[57]F. M. F. de Groot, M. Grioni, J. C. Fuggle, J. Ghijsen, G. A. Sawatzky, and H. Petersen, Phys. Rev. B **40**, 5715 (1989).

[58]We note that the multiplet simulations at the Co L_3 and L_2 edges illustrated above already indicate that the IS configurations cannot be a significant species in the systems under study here.

[59]For a most concise and clear illustration of hopping processes between neighboring Co sites, spin-up and spin-down states of the e_g and the t_{2g} orbitals are displayed at the same energy level. In principle, these states are split by (i) the (noncubic) crystal field and (ii) the (Hund's rule) exchange interaction.

[60]A. Maignan, V. Caignaert, B. Raveau, D. Khomskii, and G. Sawatzky, Phys. Rev. Lett. **93**, 026401 (2004).

[61]M. A. Señarís-Rodríguez and J. B. Goodenough, J. Solid State Chem. **118**, 323 (1995).

[62]The complete picture of the configuration fluctuation model is outlined in Ref. 61: "In a configuration fluctuation, the Co^{3+} LS ions transfer two t_{2g} electrons equally to each of the six neighboring Co^{3+} HS ions and a Co^{3+} HS ion transfers back two e_g electrons equally to each of the six neighboring Co^{3+} LS ions, to give no net transfer of charge but an interchange of spin states."

[63]Alternatively, the ferromagnetism might be explained in terms of a ferromagnetic superexchange via virtual t_{2g} hopping processes between Co^{3+} LS and Co^{3+} HS neighbors.